Chemical and environmental stability of monazite-cheralite solid solutions Ln1-2Ca Th PO4 (Ln = Pr, Nd; x = 0–0.15): A thermodynamic study

Danwen Qin, Anna Shelyug, Stéphanie Szenknect, Adel Mesbah, Nicolas Clavier, Nicolas Dacheux, Alexandra Navrotsky

Chemical and environmental stability of monazite-cheralite solid solutions $Ln_{1-2x}Ca_xTh_xPO_4$ (Ln = Pr, Nd; x = 0 – 0.15): a thermodynamics study

Danwen Qin[1,2], Anna Shelyug[3*], Stéphanie Szenknect[1*], Adel Mesbah[1,4], Nicolas Clavier[1], Nicolas Dacheux[1] and Alexandra Navrotsky[5]

[1] ICSM, Univ Montpellier, CEA, CNRS, ENSCM, Bagnols sur Cèze, France

[2] Sino-French Institute of Nuclear Engineering and Technology, Sun Yat-Sen University, 519082 Zhuhai, China

[3] Institute of Solid State Chemistry, Yekaterinburg 620990, Russia

[4] Univ Lyon, Université Claude Bernard Lyon 1, CNRS, UMR 5256, Institut de Recherches sur la Catalyse et L'Environnement de Lyon (IRCELYON), Villeurbanne, France

[5] School of Molecular Sciences and Navrotsky Eyring Center for Materials of the Universe, Arizona State University, Tempe AZ 85287, U.S.A.

* Corresponding authors: ashelyug@ucdavis.edu; stephanie.szenknect@cea.fr

ABSTRACT

Monazite-cheralite ceramics are a promising waste form for actinides. To elucidate the long-term behavior of this matrix in aqueous solutions, this study measured thermodynamic data for Th-rhabdophanes $Ln_{1-2x}Ca_xTh_xPO_4 \cdot nH_2O$ (with Ln = Pr, Nd; x = 0 – 0.15) and the associated anhydrous monazite-cheralites $Ln_{1-2x}Ca_xTh_xPO_4$. Solubility experiments at 298 K and high temperature oxide melt solution calorimetry were combined for calculation of ΔG_f°, ΔH_f° and S_m° of Th-rhabdophanes and associated monazite-cheralites. Standard solubility constants were employed in a geochemical simulation using the PHREEQC software, the results of which confirmed the high chemical stability of the monazite-cheralite phases and supported their use as a specific conditioning matrix for the long-term immobilization of actinides.

Keywords: thorium, rhabdophane, monazite, cheralite, solubility, calorimetry, stability.

1 Introduction

Monazite-cheralite $Ln_{1-2x}Ca_xAn^{IV}_xPO_4$ (Ln = La-Gd, An = Th, U, Np, Pu) solid solutions are promising radioactive waste matrices for the specific conditioning of actinides, as they adopt the monazite crystal structure (monoclinic, $P2_1/n$), which provides high chemical stability, considerable tetravalent actinide capacity, and good resistance to auto-irradiation (Dacheux et al., 2013). Indeed, monazites are repeatedly reported as being able to accumulate and immobilize actinides (U/Th) and their daughter products within their structure even after multiple sedimentations and metamorphic cycles (> 10^9 y) in the geologic environment (Boatner, 2002). Moreover, no chemical alteration of monazite has been observed during weathering, erosion and transport processes, which only lead to mechanical abrasion (Montel et al., 2000; Montel et al., 2011). Such excellent chemical durability could be explained from both kinetic and thermodynamics points of view. The studies on the dissolution kinetics of monazites report their low dissolution rates (Gausse, 2016; Gausse et al., 2018). Even under extreme conditions, the normalized dissolution rate of $LnPO_4$ (Ln = La, Ce, Nd, and Gd) is lower than that of borosilicate glass R7T7, the reference material for high-level waste conditioning (*i.e.* 4.0×10^{-3} g m^{-2} d^{-1} at 363 K in 0.1 mol L^{-1} HNO_3 (Gausse, 2016; Gausse et al., 2018) compared to 1 g m^{-2} d^{-1} at 363 K in deionized water (Delage and Dussossoy, 1990), respectively).

In addition to the high resistance to dissolution, it is essential to guarantee the thermodynamic stability of monazite-cheralite in groundwater. Upon leaching in groundwater, the forming phases might precipitate on the surface of the material limiting further release of radionuclides. For monazite end-members, the nature of the neoformed phase is temperature-dependent (Du Fou de Kerdaniel et al., 2007a; Du Fou de Kerdaniel et al., 2007b). As reported by Du Fou de Kerdaniel et al. (2007b), below a particular temperature (363 K for La, 383 K for Ce, 393 K for Pr) this phase is a hydrated phosphate compound, rhabdophane $LnPO_4 \cdot 0.667H_2O$ (monoclinic C2) (Mesbah et al., 2014), while at higher temperature, the solubility-controlling phase might be monazite itself. Indeed, the reprecipitation of rhabdophane at low temperature was observed during monazite dissolution tests, resulting in a decrease of the leaching rate of lanthanides after the initial stage of dissolution (Du Fou de Kerdaniel, 2007; Du Fou de Kerdaniel et al., 2007b; Gausse et al., 2018).

For tetravalent actinide bearing phosphates (*e.g.* monazite-cheralite), the solubility-controlling phases for tetravalent actinide may be more complex. Du Fou de Kerdaniel (2007) observed a decrease of the leaching rate during dissolution of several phosphate ceramics (*i.e.* (Nd,Th)-britholite $NdCa_9Nd_{1-x}Th_x(PO_4)_{5-x}(SiO_4)_{1+x}$, monazite-cheralite $Ln_{1-2x}Ca_xAn^{IV}_xPO_4$ (An = Th, U), thorium phosphate diphosphate β-$Th_4(PO_4)_4P_2O_7$, noted as β-TPD, and associated β-TPD/monazite composites. In this study, SEM images confirmed the formation of a mixture of rhabdophane $Nd_{1-2x}Ca_xTh_xPO_4 \cdot 0.5H_2O/GdPO_4 \cdot nH_2O$, $SiO_2 \cdot nH_2O$, and $(U, Th)_2(PO_4)_2(HPO_4) \cdot H_2O$ (TPHPH-type solids) on the surface of the sintered pellet. Therefore, Th-rhabdophane, and TPHPH are potential solubility-controlling phases during the leaching process of Th-monazite-cheralite. Consequently, there is great interest to determine the thermodynamic properties of these phases, leading to clarification of the mechanism and driving force governing the solubility of tetravalent actinides and lanthanides.

Several studies have investigated the solubility of hydrated lanthanide or actinide phosphates, such as rhabdophane and TPHPH) (Clavier, 2004; Clavier et al., 2006; Gausse et al., 2016; Jonasson et al., 1985; Qin et al., 2017a; Robisson et al., 2002). Their results suggest these compounds exhibit low Th solubility. Clavier (2004) first reported that the solubility constant,

$\lg K^{\circ}_{s,0}$ associated with TPHPH reached -66.4 ± 1.1 (Clavier, 2004; Clavier et al., 2006). More recently, this value was refined to -71.2 ± 1.3 (Qin et al., 2017a). When saturation experiments were performed in 1 mol L^{-1} HNO_3, the thorium concentration was found to be (1.9 ± 0.1) × 10^{-3} mol L^{-1}. Gausse et al. (2016) determined the solubility of the $LnPO_4 \cdot nH_2O$ series (Ln = La-Gd) from under- and super-saturation experiments to range from -24.1 ± 0.3 to -25.8 ± 0.3. The obtained lanthanide concentrations when saturation conditions were reached (in 0.1 mol L^{-1} HNO_3) were about 1 × 10^{-3} mol L^{-1}. Due to the interplay between rhabdophane and monazite mentioned above, the determination of the solubilities of monazite end-members $LnPO_4$ (Ln = La-Gd) should take place under hydrothermal conditions (T = 373 – 523 K). Recently, Gysi et al., (2018) and Van Hoozen et al. (2020) have determined the solubility products of monazite end-members $LnPO_4$ (Ln = La-Gd) ranging from -27.7 ± 0.1 to -32.3 ± 0.1. The concentration of Ln at equilibrium was lower than 1.1 × 10^{-4} mol L^{-1} in 0.01 mol L^{-1} $HClO_4$.

To investigate the behavior of monazite-cheralite at various temperatures, besides solubility experiments, it is essential to determine thermodynamics of formation of all structures in the system. Recently, the enthalpy of formation of rhabdophanes and the related monazites were determined with the application of high temperature oxide melt solution calorimetry (Shelyug et al., 2018). This study further suggested that Ln-rhabdophane ($LnPO_4 \cdot nH_2O$; Ln = La-Gd) was thermodynamically metastable with respect to the corresponding monazite plus water at all temperatures under 0.1 MPa water pressure Another thermodynamic study of hydrated phosphates adopting the churchite structure ($LnPO_4 \cdot 2H_2O$; Ln = Gd-Lu) also confirmed its stability in the case of aqueous alteration of xenotimes, delaying the release of contained actinides into the environment (Subramani et al., 2019).

The present study evaluates the stability of Th-rhabdophanes $Ln_{1-2x}Ca_xTh_xPO_4 \cdot nH_2O$ (Ln = Pr, Nd; x = 0 – 0.15) and corresponding monazite-cheralite solid solutions. These compositions were chosen to fulfill critical requirements of ceramic wasteform for the specific conditioning of actinides such as the capability to incorporate up to 10 wt.% of highly radioactive actinides within their structure. The saturation phenomenon were demonstrated, providing means for determination of the solubility constants of the formed phases. Enthalpies of formation were obtained by high temperature oxide melt solution calorimetry. Combining these results, the ΔG°_f, ΔH°_f and S°_m values for Th-rhabdophane/monazite-cheralite solid solution were determined and used in simulations using PHREEQC software, leading to a better understanding of the chemical stability of these materials from a thermodynamic point of view.

2 Materials and methods

2.1 Preparation and initial characterization of Th-rhabdophane precursors, $Ln_{1-2x}Ca_xTh_xPO_4 \cdot nH_2O$ (Ln = Pr, Nd) and associated monazite-cheralite, $Ln_{1-2x}Ca_xTh_xPO_4$.

The Th-rhabdophanes $Pr_{1-2x}Ca_xTh_xPO_4 \cdot nH_2O$ (x = 0 – 0.15) and $Nd_{0.8}Ca_{0.1}Th_{0.1}PO_4 \cdot nH_2O$ were synthesized according to the hydrothermal protocol reported in a previous study (Qin et al., 2017b). The metal salts used as staring materials were analytical grade and provided by Sigma-Aldrich: $PrCl_3 \cdot 6H_2O$ (99.9%), $NdCl_3 \cdot 6H_2O$ (99.9%), $CaCl_2 \cdot nH_2O$, $Th(NO_3)_4 \cdot 4\text{-}5H_2O$. $PrCl_3$, $NdCl_3$ and $CaCl_2$ were dissolved in 0.1M HCl and $Th(NO_3)_4 \cdot 4\text{-}5H_2O$ in 4M HNO_3. The acids above were prepared from concentrated HCl (37%, Carlo Erba) and HNO_3 (69.5%, Carlo Erba). The final concentration of each cation was determined in solution by inductively coupled plasma – optical

emission spectrometry (ICP-OES) and was about 0.5 M for $PrCl_3$, $NdCl_3$, and $Th(NO_3)_4$·while about 1.5 M for $CaCl_2$.

Then, lanthanide, thorium and calcium solutions were weighed and mixed into a Teflon container. The Ln and Th cations were introduced in the proportion expected in the solid phase, whereas the stoichiometric ratio Ca/Th in the mixture was equal to 10. Then, 5 mol L^{-1} H_3PO_4 solution was added to the mixture of cations in order to obtain an excess of 3 mol. % of P with respect to (Ln + Th). The solution was stirred for 15 min and the Teflon container was placed in a Parr autoclave. The hydrothermal treatment was performed at 383 K in oven during 4 days. Then, the obtained precipitate was washed twice in water then once in ethanol and dried at 363 K overnight. Once the Th-rhabdophane powders were obtained, a part of the samples was calcined at 1373 K for 6 h to obtain the associated monazite-cheralite solid solutions, $Ln_{1-2x}Ca_xTh_xPO_4$ (Ln = Pr, Nd; x = 0 – 0.15) or $Nd_{0.8}Ca_{0.1}Th_{0.1}PO_4$.

The obtained powders were all characterized with powder X-ray diffraction (PXRD) on a Bruker D8 Advance diffractometer equipped with copper radiation (Cu $K\alpha_{1,2}$, λ=1.54184 Å) using reflection geometry. The powders were placed in a special sample holder to avoid any radioactive contamination. Each PXRD pattern was collected from 5 to 100 ° (2θ) with a Δθ step of 0.019 °. For each step, the collection time was 3.68 s, resulting in a total counting time of about 3 hours. The PXRD patterns confirmed the single-phase nature of the rhabdophane and monazite-cheralite samples (see ***Figure S1*** of ***Supporting Information***).

In order to determine the actual stoichiometry of the prepared Th-rhabdophanes, about 20 mg of the powders were fully dissolved in 2.5 mL fresh aqua regia. Once the dissolution was completed, these solutions were diluted with 0.16 mol L^{-1} HNO_3 solution so that the elemental concentration of lanthanide was about 15 mg L^{-1}. The elemental concentrations of Th, P, Ca, and Ln were then determined by ICP-OES on a Spectro Arcos EOP. Prior to analysis, the ICP-OES instrument was calibrated. The calibration solutions were obtained by dilution of commercially available SPEX standard solutions ($C_{initial}$ = 1000 mg L^{-1}) using 0.16 mol L^{-1} HNO_3. The concentrations series of the calibration solutions for all elements of interest were fixed at 0, 0.25, 0.5, 0.75, 1, 2.5, 5, 10, and 20 mg L^{-1} ($C_{Ca} = C_{Th} = C_{Nd} = C_P$). For each element, four recommended wavelengths were considered. The calibration for a wavelength was considered valid if the coefficient of determination for the calibration curve, R^2, was over 0.999. The measurement was considered reliable if the relative error between the values reported from different wavelengths was lower than 5 %. Following this protocol, the detection limits were 2.5 mg L^{-1} for Ca, 0.25 mg L^{-1} for Th and Nd, and 1 mg L^{-1} for P. The elemental concentration in solution was then calculated as the average of the values obtained for each emission wavelength. The standard error was estimated as twice the standard deviation. The chemical composition of the samples are listed in **Table 1**. Since as-prepared monazite-cheralite powders only partially dissolved in fresh aqua regia, the proportions of elements of interest were considered the same as in their Th-rhabdophane precursors.

The water content in Th-rhabdophane samples was determined by thermogravimetric analysis coupled with differential scanning calorimetry (TGA-DSC) in a Netzsch STA 449C. About 15 – 20 mg of the powdered Th-rhabdophane sample were placed in a platinum crucible and were heated under 40 mL min^{-1} flow of air to 1273 K at a rate of 10 K min^{-1}. Empty crucible was used as a reference during baseline run prior to the experiment to correct for the drift in weight as a function of temperature. The calibration of the instrument's heat flow was performed against the heat capacity of a sapphire disk.

Table 1. Chemical composition (cationic mole ratios) of the rhabdophane samples $Ln_{1-2x}Ca_xTh_xPO_4 \cdot nH_2O$, determined by ICP-OES after complete dissolution.

Sample name	Ln	Ca	Th
$Pr_{0.9}Ca_{0.05}Th_{0.05}PO_4 \cdot nH_2O$	0.892	0.049	0.059
$Pr_{0.8}Ca_{0.10}Th_{0.10}PO_4 \cdot nH_2O$	0.785	0.111	0.105
$Pr_{0.7}Ca_{0.15}Th_{0.15}PO_4 \cdot nH_2O$	0.697	0.150	0.143
$Nd_{0.8}Ca_{0.10}Th_{0.10}PO_4 \cdot nH_2O$	0.804	0.109	0.086

2.2 $Nd_{0.8}Ca_{0.10}Th_{0.10}PO_4$ solubility experiments

Solubility experiments were conducted starting from under-saturated conditions. For each experiment, about 100 mg of $Nd_{0.8}Ca_{0.10}Th_{0.10}PO_4$ was placed in a 120 mL Savillex jar containing 100 mL of 1, 0.32, or 0.1 mol L^{-1} HNO_3 solution. These solutions were prepared by dilution of 15 mol L^{-1} HNO_3 (69.5 %, Carlo-Erba). These jars were placed in a VWR incubating mini shaker at 298 K during the entire leaching process. 5 mL of solvent were regularly extracted from the jar and were centrifuged for the measurement of Ca, Th, Nd, and P elemental concentrations by ICP-OES. As the dissolution vessels were considered as closed systems, the elemental concentrations stabilized if a saturation equilibrium was reached once three consecutive analyses of the Th, Nd, and P concentrations were not significantly different (relative error ≤ 5 %). The Nd, Th and P concentrations at equilibrium were calculated as the average of the last concentrations measurements that were not significantly different by considering the experimental uncertainty. Then, the uncertainty on the elemental concentrations at equilibrium was determined as twice the standard deviation of the selected consecutive measurements. As the monazite matrix exhibited a low solubility and as Ca was a minor component in the powder (about only 2 wt.%), its elemental concentration was close to the detection limit of ICP-OES ($C_{Ca} \leq 2.5$ mg L^{-1}) leading to a large uncertainty on the determined concentration. For experiments performed in the less acidic media, the elemental concentration in Ca was thus calculated assuming that the dissolution was stoichiometric. Then, these elemental concentration values as well as the proton activity were used to calculate the standard solubility constant of monazite-cheralite $Nd_{0.8}Ca_{0.10}Th_{0.10}PO_4$.

2.3 Calculation of standard solubility constant of $Nd_{0.8}Ca_{0.10}Th_{0.10}PO_4$

PHREEQC simulations (version 3.3.8.11728) (Parkhurst and Appelo, 2013) were performed in order to calculate the activities of Ca^{2+}, Nd^{3+}, Th^{4+} and H_3PO_4 in the 1, 0.32, and 0.1 mol L^{-1} HNO_3 solutions from the elemental concentrations at equilibrium. ThermoChimie database (version 10a) (Giffaut et al., 2014) was employed. The complexation constants of the inorganic species in this database were mostly selected from internationally recognized thermodynamic databases. Especially, it included the data of thorium species published by NEA-OECD's Thermochemical Database (TDB) project (Rand et al., 2009). However, the data associated to neodymium species were not included in the ThermoChimie database. In order to solve this problem, the thermodynamic data of neodymium inorganic complexes were selected from one of the other well-recognized database (LLNL-TDB) (Lawrence Livermore National Laboratory TDB) (Johnson et al., 2000). Moreover, since rhabdophane $NdPO_4 \cdot 0.667H_2O$ and $Th_2(PO_4)_2(HPO_4) \cdot H_2O$ (TPHPH) are considered potentially forming phases during the solubility experiments, their solubility constant

values, evaluated in the previous works (Gausse et al., 2016; Qin et al., 2017a), were introduced in the used database as well.

The solubility tests were conducted in acidic conditions (*i.e.*, pH = 0 – 1) because of the very high chemical durability of the materials. However, only a small amount of monazite solid was dissolved during the whole test, *e.g.*, less than 7 mg of sample when making the test in 100 mL of 1 mol L^{-1} HNO_3. This result suggests that the concentration of HNO_3 can be considered as unchanged and that the pH value can be deduced from the initial concentration of HNO_3. The method used to calculate the pH is described in the ***Supporting Information***. The obtained values of pH were equal to 0.13 ± 0.02, 0.63 ± 0.02 and 1.10 ± 0.02 for 0.1, 0.32 and 1 mol L^{-1} HNO_3, respectively.

A protonation equilibrium is involved in the dissolution reaction.

$$Nd_{0.8}Ca_{0.1}Th_{0.1}PO_4 + 3\ H^+ \rightleftarrows 0.8\ Nd^{3+} + 0.1\ Ca^{2+} + 0.1\ Th^{4+} + H_3PO_4 \quad (1)$$

Therefore, the solubility product of the monazite-cheralite solid solution ${}^*K_s$ can be defined as follows:

$${}^*K_s(\text{monazite} - \text{cheralite}) = \frac{[Nd^{3+}]^{0.8}[Ca^{2+}]^{0.1}[Th^{4+}]^{0.1}[H_3PO_4]}{[H^+]^3} \quad (2)$$

where [i] denotes the molarity of species (expressed in mol L^{-1}).

The conversion between molarity and molality, m_i (mol kg_w^{-1}), was done using the following expression:

$$m_i = \frac{1000\ [i]}{1000\ \rho - [i]\ M_i} \quad (3)$$

where ρ (kg L^{-1}) is the density of the solution, and M_i(g mol^{-1}) is the molar mass of species, *i*. The density of HNO_3 solutions was calculated using the model proposed by Novotny and Söhnel (Novotny and Sohnel, 1988) (see ***Table S1*** of ***Supporting Information***).

The solubility product, expressed as a function of the molalities, ${}^*K_s^m$, is given below:

$${}^*K_s^m(\text{monazite-cheralite}) = \frac{m_{Nd^{3+}}^{0.8} \times m_{Ca^{2+}}^{0.1} \times m_{Th^{4+}}^{0.1} \times m_{H_3PO_4}}{m_{H^+}^3} \quad (4)$$

The standard solubility constant of the monazite-cheralite $Nd_{0.8}Ca_{0.10}Th_{0.10}PO_4$ is defined as:

$${}^*K_s^\circ(\text{monazite-cheralite}) = \frac{(Nd^{3+})^{0.8} \times (Ca^{2+})^{0.1} \times (Th^{4+})^{0.1} \times (H_3PO_4)}{(H^+)^3} \quad (5)$$

where (i) denotes the activity of species, *i*.

The Specific Ion interaction Theory (SIT) was used to estimate the activity coefficient, γ_i, that relates the activity of the species, (i) to its molality, m_i (Ciavatta, 1980). The lg γ_i was evaluated as:

$$\lg \gamma_i = -z_i^2 D + \Sigma_j \varepsilon(i,j) m_j \quad (6)$$

where, z_i is the charge of species *i*, ε(i, j) is the interaction coefficient between ion *i* and counter-ion *j* (see **Table S2** of ***Supporting Information***) and D is the term of Debye-Hückel expressed as:

$$D = \frac{A\sqrt{I_m}}{1+Ba_j\sqrt{I_m}} \quad (7)$$

where, A and B are temperature and pressure dependent constants, and a_j is an ion size parameter for the hydrated ion, *j*. The value of the Debye-Hückel limiting slope, A, is (0.509 ± 0.001) $kg^{½}\ mol^{-½}$ at 298 K and 1 bar. The recommended Ba_j value is equal to 1.5 $kg^{½}\ mol^{-½}\ m^{-1}$ at 298 K and 1 bar (Rand et al., 2009).

Combining equations (4-6) leads to following expression:

$$\lg\ {}^{*}K_s^{\circ} = \Delta z^2 D + \Delta\varepsilon\ I_m + \lg\ {}^{*}K_s^{m} \quad (8)$$

where ΔX stands for $\Sigma_i \nu_i X_i$.

The $\Delta\varepsilon$ term in equation (8) was simplified by considering only the interactions between the ions participating in the reaction and the ions of the electrolyte solution. This approximation could be done because the ions of the electrolyte solution have concentrations much higher than those participating in the reaction. Moreover, the $\varepsilon(i,j)$ value for ions with the same charge sign is equal zero. It is also null for uncharged species.

The standard solubility constants $K_{s,0}^{\circ}$ were also calculated by using PO_4^{3-} species:

$$K_{s,0}^{\circ}\ (\text{monazite-cheralite}) = \left(Nd^{3+}\right)^{0.8} \times (Ca^{2+})^{0.1} \times \left(Th^{4+}\right)^{0.1} \times \left(PO_4^{3-}\right) \quad (9)$$

It is worth noting that $K_{s,0}^{\circ}$ can be deduced from ${}^{*}K_s^{\circ}$ according to:

$$K_{s,0}^{\circ} = {}^{*}K_s^{\circ} \times K_{a1} \times K_{a2} \times K_{a3} \quad (10)$$

where, K_{a1}, K_{a2}, K_{a3} are the phosphoric acid constants at 298 K related to $H_3PO_4/H_2PO_4^-$ (pK_{a1} = 2.14), $H_2PO_4^-/HPO_4^{2-}$ (pK_{a2} = 7.212), and HPO_4^{2-}/PO_4^{3-} (pK_{a3} = 12.35), respectively (see **Table S3** of ***Supporting Information***).

Several neoformed phases such as rhabdophane, TPHPH, Th-rhabdophane, $Nd_{0.8}Ca_{0.10}Th_{0.10}PO_4 \cdot nH_2O$ or the monazite-cheralite $Nd_{0.8}Ca_{0.10}Th_{0.10}PO_4$ itself could act as solubility-controlling phase in our experiments. Indeed, Shelyug *et al.* (Shelyug et al., 2018) already reported the Gibbs free energy of reaction from rhabdophane $NdPO_4 \cdot 0.746H_2O$ to monazite $NdPO_4$ plus water at 298 K as -9.1 ± 9.5 kJ mol^{-1}. As the Gibbs free energy at 298 K is close to 0 taking into account the uncertainty associated to this value, monazite $NdPO_4$ appears as stable as rhabdophane $NdPO_4 \cdot nH_2O$. The Gibbs free energy of the reaction from $Nd_{0.8}Ca_{0.10}Th_{0.10}PO_4 \cdot nH_2O$ to monazite-cheralite $Nd_{0.8}Ca_{0.10}Th_{0.10}PO_4$ plus water could be also close to zero, which would mean that both Th-rhabdophane and monazite-cheralite could act as the solubility controlling-phase.

Assuming that the Th-rhabdophane is the phase that controls the equilibrium, the dissolution-precipitation of $Nd_{0.8}Ca_{0.10}Th_{0.10}PO_4 \cdot nH_2O$ at pH = 0 – 1 can be written as follows:

$$Nd_{0.8}Ca_{0.1}Th_{0.1}PO_4 \cdot nH_2O + 3\ H^+ \rightleftarrows 0.8\ Nd^{3+} + 0.1\ Ca^{2+} + 0.1\ Th^{4+} + H_3PO_4 + n\ H_2O \quad (11)$$

Thus, the standard solubility constant ${}^{*}K_s^{\circ}$ of $Nd_{0.8}Ca_{0.10}Th_{0.10}PO_4 \cdot nH_2O$ rhabdophane can be calculated as:

$$^{*}K_s^{\circ}(\text{rhabdophane}) = \frac{\left(Nd^{3+}\right)^{0.8} \times \left(Ca^{2+}\right)^{0.1} \times \left(Th^{4+}\right)^{0.1} \times (H_3PO_4) \times (H_2O)^n}{\left(H^+\right)^3} \quad (12)$$

The standard solubility constants $K_{s,0}^{\circ}$ were also calculated by using PO_4^{3-} species:

$$K_{s,0}^{\circ}\,(\text{rhabdophane}) = \left(Nd^{3+}\right)^{0.8} \times (Ca^{2+})^{0.1} \times \left(Th^{4+}\right)^{0.1} \times \left(PO_4^{3-}\right) \times (H_2O)^n \quad (13)$$

Thus, the difference between the values of $K_{s,0}^{\circ}$(rhabdophane) and of $K_{s,0}^{\circ}$(monazite-cheralite) can be expressed as:

$$\lg K_{s,0}^{\circ}(\text{rhabdophane}) = \lg K_{s,0}^{\circ}(\text{monazite-cheralite}) + n \times \lg (H_2O) \quad (14)$$

The activity of water in HNO_3 can be calculated from:

$$\lg(H_2O) = -\frac{2 \times m_{HNO_3} \times \phi_m}{\ln 10 \times 55.508} \quad (15)$$

where ϕ_m is the osmotic coefficient of the mixture and 55.508 mol kg^{-1} is the molality of pure water. Lewis and Randall (Lewis et al., 1961) have given a general formula to determine the osmotic coefficient for an ionic medium with concentration much larger than those of the reacting ions. Therefore, the osmotic coefficient of the HNO_3 solutions can be calculated as follows:

$$1 - \phi_m = \frac{A \times \ln 10}{I_m \times (Ba_j)^3}\left[1 + Ba_j\sqrt{I_m} - 2 \times \ln\left(1 + Ba_j\sqrt{I_m}\right) - \frac{1}{1 + Ba_j\sqrt{I_m}}\right] - 0.5 \times \ln 10 \times \varepsilon\left(H^+, NO_3^-\right) \times m_{HNO_3} \quad (16)$$

2.4 High-temperature oxide melt solution calorimetry

Rhabdophane and monazite-cheralite samples were all submitted to high-temperature oxide melt solution calorimetry. The experiments were performed in a custom-built Tian-Calvet twin calorimeter (Navrotsky, 1977, 2014). The methodology was the same as in the earlier studies of rhabdophane end-members $LnPO_4 \cdot nH_2O$ (Shelyug et al., 2018) and other materials (Hirsch et al., 2017; Neumeier et al., 2017). About 5 mg of the sample powder was pressed into pellet and dropped into molten lead borate ($2PbO\text{-}B_2O_3$) kept in a Pt crucible inside the cell at 1073 K. The cell was flushed (40 mL min^{-1}) and the solvent was bubbled (4.5 mL min^{-1}) with oxygen to remove the water vapor from the cell and to promote dissolution. The measured signal of heat flow over time was integrated using CALISTO (Setaram) software to calculate the enthalpy of drop solution. Eight measurements were taken for each sample to collect statistics.

3 Results and Discussion

3.1 Solubility experiments

The evolution of elemental concentrations during the leaching of monazite-cheralite $Nd_{0.8}Ca_{0.10}Th_{0.10}PO_4$ in 1 mol L^{-1} HNO_3 is presented in **Figure 1a**. The elemental concentrations increased gradually, and then reached a plateau after about 200 days, which suggested the establishment of thermodynamic equilibrium. The elemental concentrations determined at thermodynamic equilibrium are listed in **Table 2**. The evolution of Th, Nd and P concentrations stated the stoichiometric dissolution of the monazite-cheralite within the experimental error (*i.e.*

[Th]/[P] = 0.17 ± 0.02, [Nd]/[P] = 0.74 ± 0.05, [Ca]/[P] = 0.12 ± 0.04 and Σ[cations]/[P] = 1.0 ± 0.4). This result suggested that stoichiometric saturation occurred and that the composition of the monazite-cheralite remained invariant during the experiment. The Ca concentration showed significant fluctuations due to the higher detection limit of ICP-OES for this element and/or potential contamination. The thorium concentration was equal to $(2.7 \pm 0.1) \times 10^{-5}$ mol L^{-1} and the associated relative mass loss reached 6.3 ± 0.3 % of the initial Th in monazite-cheralite (**Table 2**). These values were obtained in the most acidic solution (*i.e.* 1 mol L^{-1} HNO_3) confirming its strong chemical durability.

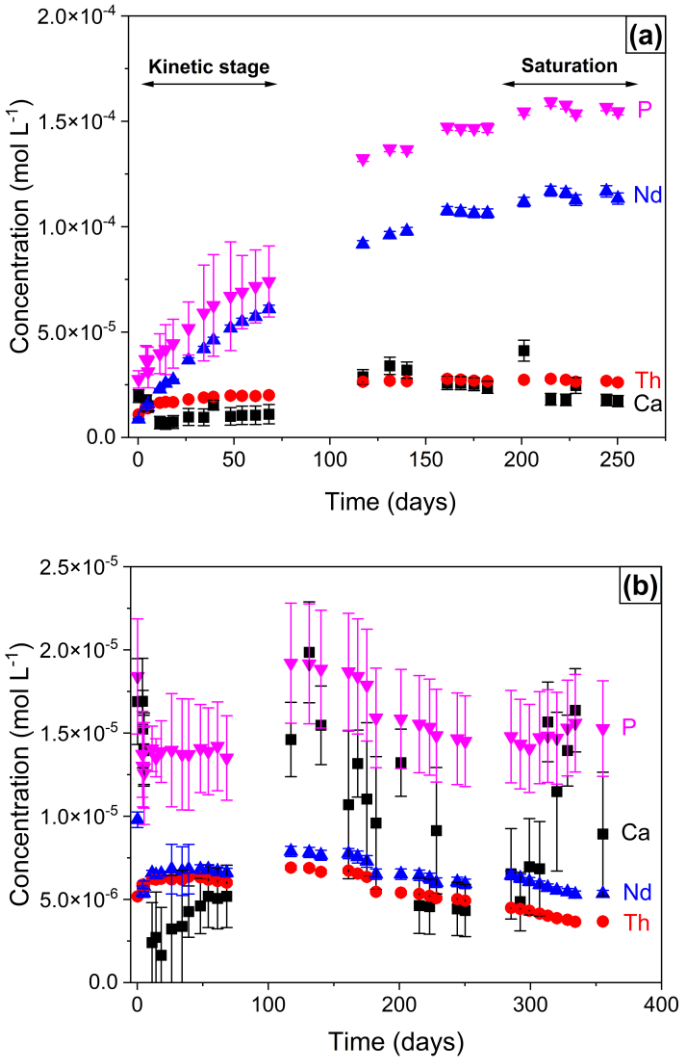

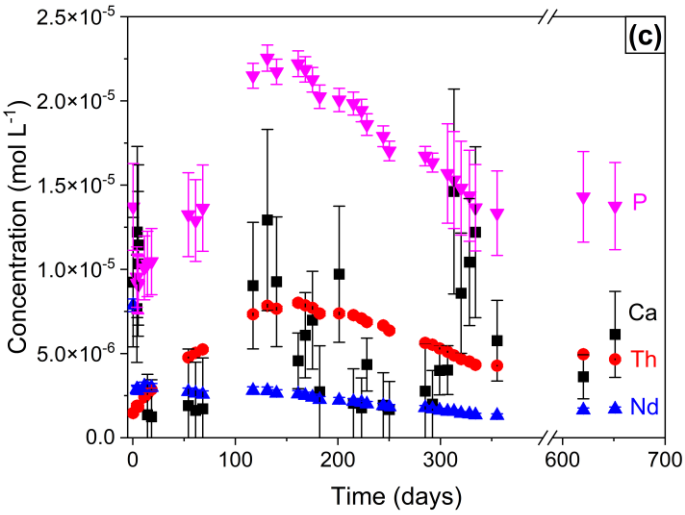

Figure 1. Evolution of elemental concentrations obtained during the leaching of $Nd_{0.8}Ca_{0.10}Th_{0.10}PO_4$ in 1 mol L^{-1} (a), 0.32 mol L^{-1} (b) and 0.1 mol L^{-1}(c) of HNO_3 at 298 K. C(Ca) (■), C(Th) (●), C(Nd) (▲) and C(P) (▼).

Table 2. Elemental concentrations of Ca, Th, Nd and P at equilibrium (average of the last concentrations measurements that were not significantly different, uncertainty determined as twice the standard deviation of the selected consecutive measurements), and relative mass loss of thorium obtained at the end of the solubility tests of $Nd_{0.8}Ca_{0.10}Th_{0.10}PO_4$ at 298 K.

C_{HNO_3} [mol L^{-1}]	[Ca] [× 10^{-5} mol L^{-1}]	[Th] [× 10^{-5} mol L^{-1}]	[Nd] [× 10^{-5} mol L^{-1}]	[P] [× 10^{-5} mol L^{-1}]	$\frac{m_{Th}(dissolved)}{m_{Th}(solid)}$ [%]
1.00 ± 0.02	1.9 ± 0.6	2.7 ± 0.1	11.5 ± 0.4	15.6 ± 0.5	6.3 ± 0.3
0.32 ± 0.01	1.0 ± 0.9	0.5 ± 0.2	0.6 ± 0.2	1.6 ± 0.4	1.0 ± 0.5
0.10 ± 0.01	0.8 ± 0.8	0.47 ± 0.06	0.2 ± 0.1	1.4 ± 0.3	1.1 ± 0.3

For the system with 0.32 mol L^{-1} HNO_3 (**Figure 1b**), the elemental concentrations of Th, Nd, and P, first increased gradually and reached a maximum after about 100 days. Then, the concentrations decreased slowly to reach a plateau after about 350 days. The rate of release of the elements was lower and the concentration at equilibrium was lower by one order of magnitude than in 1 mol L^{-1} HNO_3. Likewise, when 0.1 mol L^{-1} HNO_3 was used, the evolution of elemental concentrations was even slower than that reported in 0.32 mol L^{-1} HNO_3. The maximum of the concentrations took place at about 150 days whereas the equilibrium was reached after 600 days. In both cases, the evolution of the concentrations indicated that the dissolution of the monazite-cheralite was not stoichiometric. The shape of the curves suggested that super-saturated conditions were attained before the precipitation of a phase incorporating all the elements released in solution. However, even if the proportion of Th in the solution was considered to be over-stoichiometric compared to the initial powder, only 1 % of Th was released in the solution (see **Table 2**). Unlike what happened in 1 mol L^{-1} HNO_3, the results obtained in 0.32 and 0.1 mol L^{-1} HNO_3 solutions clearly did not meet the criteria for stoichiometric saturation as defined in (Bruno et al., 2007). Nevertheless, we decided to calculate the monazite-cheralite standard solubility constant in the three leaching media and to compare the obtained values with the reference data obtained in 1 mol L^{-1} HNO_3.

According to the thorium loss, the amount of dissolved monazite-cheralite reached about 3×10^{-5} mol in 1 mol L^{-1} HNO_3, and 0.4×10^{-5} mol in 0.32 and 0.1 mol L^{-1} HNO_3. Based on Eq. (1), the associated consumption of H^+ was about 8×10^{-4} mol and 1×10^{-4} mol in 1 mol L^{-1} HNO_3 and in 0.32 or 0.1 mol L^{-1} HNO_3, respectively. Therefore, the proportion of H^+ consumed by the dissolution of monazite-cheralite reached 0.8 %, 0.4 % and 1.3 % of the total amount of available protons in 1, 0.32, and 0.1 mol L^{-1} of HNO_3, respectively. All these results validated the hypothesis made concerning the invariant proton concentration during the solubility experiments.

The speciation in solution was then simulated by PHREEQC considering the elemental concentrations measured at equilibrium (**Table 2**) and the calculated pH values (**Table 3**) (Parkhurst and Appelo, 2013). The calculated molalities and activities of the species of interest (*i.e.*, Ca^{2+}, Th^{4+}, Nd^{3+}, H_3PO_4) are also listed in **Table 3**.

Table 3. pH values and calculated molalities and activities of the species of interest obtained at thermodynamic equilibrium during solubility experiments of $Nd_{0.8}Ca_{0.10}Th_{0.10}PO_4$ at 298 K

C_{HNO_3} [mol L^{-1}]	pH	Molalities [× 10^{-5} mol kg^{-1}]				Activities [× 10^{-5}]			
		$m_{Ca^{2+}}$	$m_{Th^{4+}}$	$m_{Nd^{3+}}$	$m_{H_3PO_4}$	Ca^{2+}	Th^{4+}	Nd^{3+}	H_3PO_4
1.00	0.13	1.9 ± 0.6	0.049 ± 0.002	7.6 ± 0.3	14.9 ± 0.6	3 ± 1	(1.3 ± 0.1) × 10^{-4}	0.11 ± 0.01	14.9 ± 0.4
0.32	0.63	1.0 ± 0.9	0.3 ± 0.1	0.5 ± 0.1	1.5 ± 0.3	0.2 ± 0.2	(1.7 ± 0.7) × 10^{-3}	0.02 ± 0.01	1.5 ± 0.3
0.10	1.10	0.8 ± 0.8	0.32 ± 0.04	0.13 ± 0.02	1.3 ± 0.2	0.3 ± 0.3	(7 ± 1) × 10^{-3}	0.01 ± 0.01	1.3 ± 0.2

Assuming the dissolving monazite-cheralite to be the solubility-controlling phase, the values of $\lg^{*}K_s^m$ (monazite-cheralite) were calculated according to Eq. (4) as -7.8 ± 0.1, -8.2 ± 0.3, and -7.4 ± 0.2 in 1, 0.32, and 0.1 mol L^{-1} HNO_3, respectively. The $\lg^{*}K_s^{\circ}$(monazite-cheralite) values were calculated from Eq. (5) as -9.6 ± 0.1, -9.6 ± 0.3 and -8.4 ± 0.2 for 1, 0.32, and 0.1 mol L^{-1} HNO_3, respectively. According to Eq. (9), the associated values of standard solubility constant, $\lg K_{s,0}^{\circ}$ (monazite-cheralite), were -31.1 ± 0.1, -31.3 ± 0.4, and -30.1 ± 0.3, respectively. All the values obtained in the three leaching media are reported in **Table 4**.

On the contrary, if Th-rhabdophane was the solubility-controlling phase, the solubility constant could be calculated using Eq. (14). According to TG analysis, the number of water molecules in the chemical formula for this sample was 0.820. Based on Eq. (15) and (16), the values of $n \times \lg(H_2O)$ reached -0.015, -0.005 and -0.001 in 1, 0.32, and 0.1 mol L^{-1} HNO_3, respectively. Since these values were an order of magnitude smaller than the uncertainty associated with $\lg K_{s,0}^{\circ}$ (monazite-cheralite) (*i.e.* 0.1 – 0.4), it was assumed that $\lg K_{s,0}^{\circ}$(Th-rhabdophane) and $\lg K_{s,0}^{\circ}$(monazite-cheralite) were not significantly different.

The $\lg K_{s,0}^{\circ}$ values determined at pH = 0.13 and 0.63 are consistent taking into account the associated uncertainties. Meanwhile, the $\lg K_{s,0}^{\circ}$ value determined at pH = 1.10 was slightly higher than the values determined at lower pH. One explanation for this difference was that thermodynamic equilibrium could not have been attained at pH 1.1 due to the very slow decrease of the elemental concentrations in solution, or the dissolving monazite-cheralite was not the phase that controlled the elemental concentration at saturation. Thus, this value was not used in the estimation of the final $\lg K_{s,0}^{\circ}$ (Th-rhabdophane or monazite-cheralite) value at 298 K. The selected value for $\lg K_{s,0}^{\circ}$ (Th-rhabdophane or monazite-cheralite) at 298 K was -31.2 ± 0.3.

Table 4. Solubility products and standard solubility constants obtained at thermodynamic equilibrium during solubility experiments of $Nd_{0.8}Ca_{0.10}Th_{0.10}PO_4$ at 298 K in several nitric acid media.

pH	$\lg^{*}K_s^m$	$\lg^{*}K_s^\circ$	$\lg K_{s,0}^\circ$
0.13 ± 0.01	-7.8 ± 0.1	-9.6 ± 0.1	-31.1 ± 0.1
0.63 ± 0.01	-8.2 ± 0.3	-9.6 ± 0.3	-31.3 ± 0.4
1.10 ± 0.01	-7.4 ± 0.2	-8.4 ± 0.2	-30.1 ± 0.3

Once the $\lg K_{s,0}^\circ$ was determined, it was introduced into the ThermoChimie database and PHREEQC simulations were performed for the $Nd_{0.8}Th_{0.1}Ca_{0.1}PO_4$-$HNO_3$ and TPHPH+$NdPO_4 \cdot 0.667H_2O/HNO_3$ systems. The evolution of the elemental concentrations at thermodynamic equilibrium as the function of pH is presented in **Figure 2**. The results of the PHREEQC simulation of the $Nd_{0.8}Th_{0.1}Ca_{0.1}PO_4/HNO_3$ system (**Figure 2a**) were consistent with the experimental data reported in **Table 2**. However, the simulations suggested that the Nd and P elemental concentrations should be about three orders of magnitude higher than the experimental data if controlled by the TPHPH+$NdPO_4 \cdot 0.667H_2O/HNO_3$ system (**Figure 2b**). Meanwhile, if controlled by the TPHPH+$NdPO_4 \cdot 0.667H_2O/HNO_3$ system, the simulated Th concentration should be two orders of magnitude higher than that obtained at pH = 0.1. However, at pH = 1.1, the simulated Th concentration controlled by the TPHPH+$NdPO_4 \cdot 0.667H_2O/HNO_3$ system was closer to the experimental data than in the case of equilibrium with the Th-rhabdophane or monazite-cheralite. This result suggested that the solubility-controlling phase was always Th-rhabdophane $Nd_{0.8}Th_{0.1}Ca_{0.1}PO_4 \cdot nH_2O$ or monazite-cheralite $Nd_{0.8}Th_{0.1}Ca_{0.1}PO_4$ when the concentration of HNO_3 was in the range between 0.32 and 1 mol L^{-1}. However, for acid concentration equal to or lower than 0.1 mol L^{-1}, TPHPH could have formed and control the concentration of thorium. This might be another reason for incongruency between the elemental concentrations observed during the solubility experiment performed in 0.1 mol L^{-1} HNO_3. It could also explain why the $\lg K_{s,0}^\circ$ determined at pH = 1.1 was not consistent with the values obtained at pH = 0.13 and 0.63 (**Table 4**).

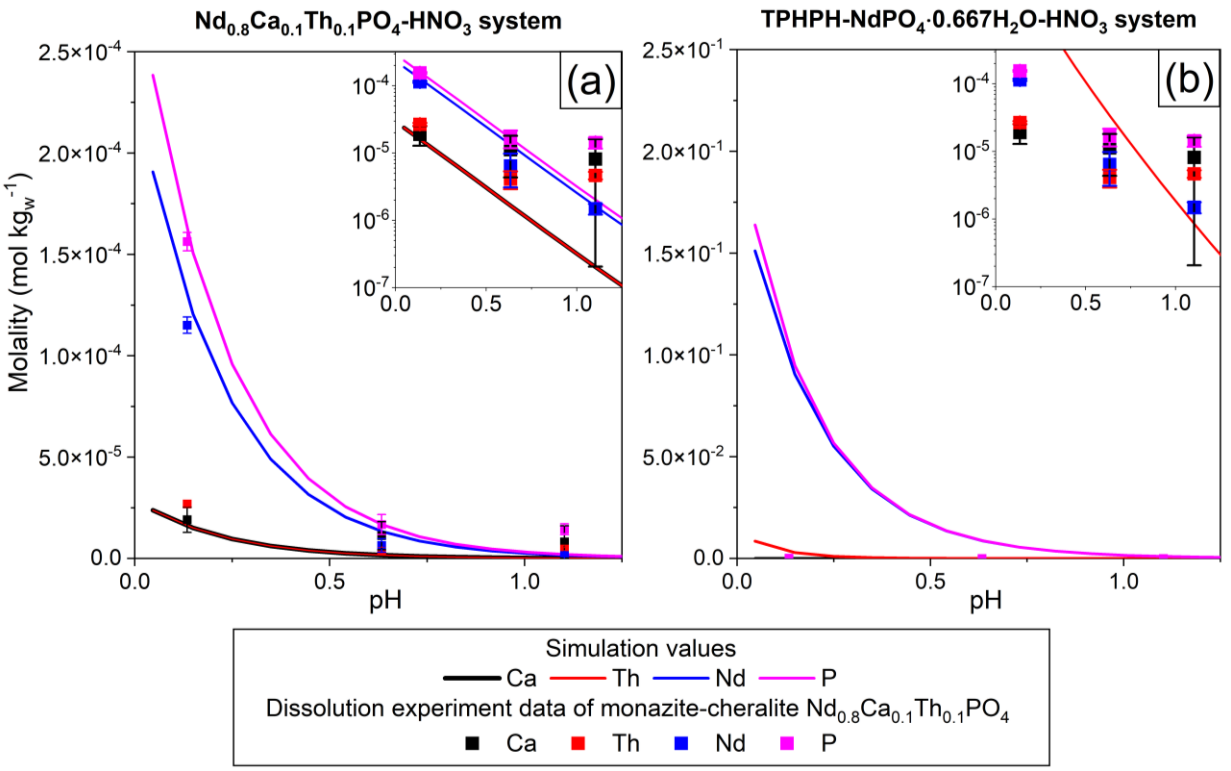

Figure 2. Evolution of elemental concentrations at thermodynamic equilibrium vs. pH and comparison of the experimental data obtained with the results of the simulations considering that the monazite-cheralite, $Nd_{0.8}Th_{0.1}Ca_{0.1}PO_4$ (a) or the $TPHPH+NdPO_4{\cdot}0.667H_2O$ (b) are the solubility controlling phases.

Finally, as the aqueous conditions in the repository site are neutral or slightly alkaline (OCDE/AEN, 1999), a complementary simulation by PHREEQC was performed from pH 0 to 8.5 in order to determine the elemental concentrations obtained when reaching saturation conditions for both $TPHPH+ThO_2+NdPO_4{\cdot}0.667H_2O/HNO_3/NaOH$ and $Nd_{0.8}Th_{0.1}Ca_{0.1}PO_4/HNO_3/NaOH$ systems (**Figure 3**). It is worth noting that in order to better simulate the contribution of other phosphate minerals to the elemental concentration in phosphorus, it was set to 10^{-6} mol L^{-1} during the whole simulation. For the first system, the thorium molality dropped below 10^{-12} mol kg_w^{-1} when the pH was above 6 and its solubility-controlling phase was ThO_2. For the second system, m_{Th} was even less than 10^{-17} mol kg_w^{-1} for pH $\geq$ 6, which was even lower than in the case where ThO_2 was the solubility-controlling phase. Consequently, by applying the $\lg K^{\circ}_{s,0}$ value determined in this study, these simulation results suggest that $Nd_{0.8}Th_{0.1}Ca_{0.1}PO_4$ has exceptional chemical stability in near neutral conditions and that using this phase as a conditioning matrix guarantees virtually no Th release in the groundwater in the long term.

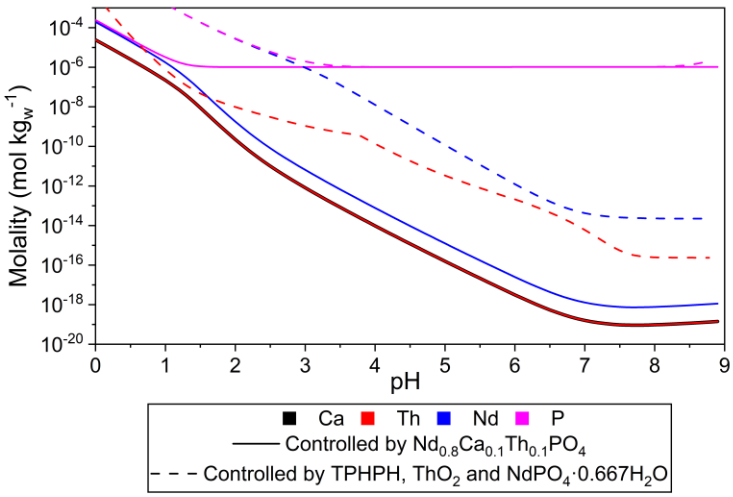

Figure 3. Molalities obtained at thermodynamic equilibrium in near neutral conditions when considering the TPHPH+ThO_2+$NdPO_4 \cdot 0.667H_2O$/HNO_3/NaOH system and the $Nd_{0.8}Th_{0.1}Ca_{0.1}PO_4$/$HNO_3$/NaOH system with $[P]_{min} = 10^{-6}$ mol L^{-1}.

3.2 High temperature calorimetry

3.2.1 Thermal behavior and data from TG-DSC analyses

Prior to further thermodynamic investigations, all samples were studied by TGA-DSC. The recorded scans are given in **Figure 4**. The first endothermic heat effect and the associated mass loss are most likely the loss of bonded water, while the exothermic peak at constant mass is the phase transition between the Th-rhabdophane and the cheralite-monazite phase. Dehydration occurred between 300 and 580 K, whereas the transition from dehydrated rhabdophane to monazite-cheralite occurred between 1000 and 1250 K. Similar processes were observed before for the Ln-rhabdophane series in Shelyug et al., (2018) and occur in the following steps:

$$\text{hydrated rhabdophane} \xrightarrow{\Delta H_{dehydr}} \text{dehydrated rhabdophane} \xrightarrow{\Delta H_{transit}} \text{cheralite} - \text{monazite} \quad (17)$$

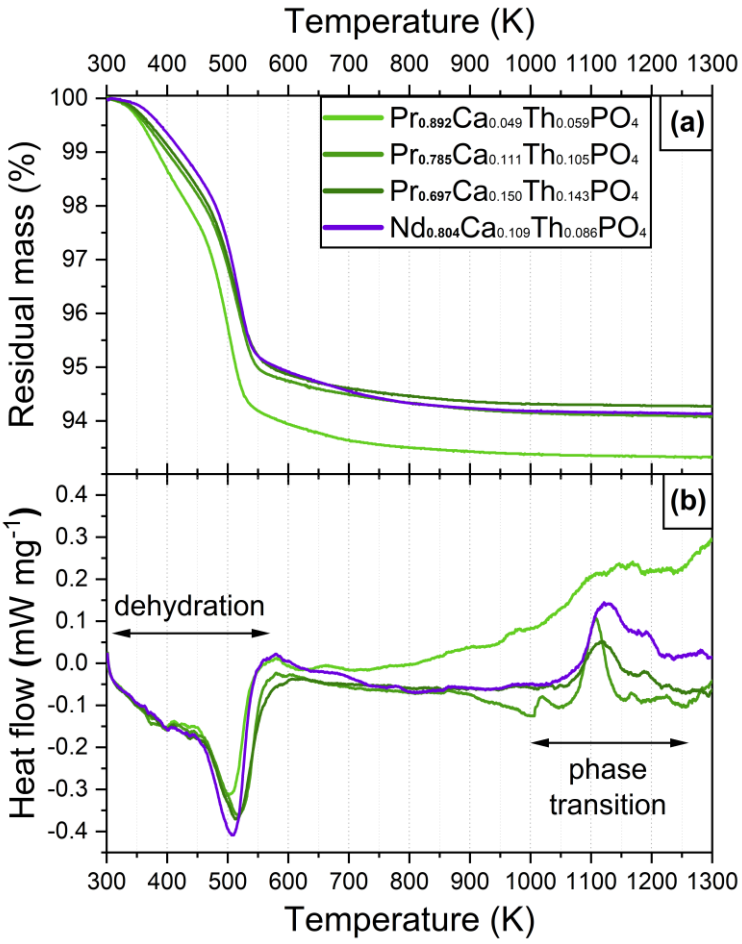

Figure 4 TGA (a) and DSC (b) scans of the Th-rhabdophane samples in this study. For simplicity, structural water (nH_2O) is omitted from samples names.

The enthalpies of dehydration, ΔH_{dehydr}, and phase transition, $\Delta H_{transit}$, can be found from direct integration of the heat flow signal and recalculated per mole of sample and are listed in **Table 5**. The water contents of the samples are calculated from water loss and are larger for the samples with higher lanthanide content considering the large ionic radius of Ln ions, which defines the size of the rhabdophane structure channels. The average enthalpy of dehydration for the samples in this study is less endothermic than that of Ln-rhabdophanes studied before (40.8 ± 0.8 vs 50.3 ± 1.4) (Shelyug et al., 2018). In order to evaluate overall stability of the monazite-cheralite solid solution in contact with water, the following reaction is considered:

$$\text{hydrated rhabdophane} \xrightarrow{\Delta H_{rh\to ch+H_2O}} \text{cheralite} - \text{monazite} + \text{water} \tag{18}$$

Its enthalpy is calculated at room temperature as:

$$\Delta H^{DSC}_{rh\to ch+H_2O} = \Delta H_{dehydr} + \Delta H_{transit} - z \times \Delta H_{vapor} \tag{19}$$

where $\Delta H_{vapor} = 44\ \text{kJ mol}^{-1}$ is the heat of water vaporization at 298 K. According to this equation, the enthalpy of reaction of Th-rhabdophane to cheralite-monazite plus water at 298 K is between -15 and -30 kJ mol^{-1}, which is slightly more exothermic compared to the values of the corresponding reaction in the Ln-rhabdophane series (Shelyug et al., 2018) meaning even less

favorable interaction of monazite-cheralite with water to form rhabdophane. This means that the incorporation of Th might strengthen the thermal stability of the monazite-cheralite solid solution.

The enthalpy of this reaction was also evaluated from the drop-solution experiments according to the equation:

$$\Delta H_{rh\rightarrow ch+H_2O} = \Delta H^{rh}_{ds,1073} - \Delta H^{ch}_{ds,1073} - z \times \Delta H_5 \quad (20)$$

and was found to be the same within experimental error as the values obtained via TGA-DSC (see **Table 5**).

Table 5. Water content and enthalpies of dehydration (ΔH_{dehydr}), phase transition ($\Delta H_{transit}$), and reaction of Th-rhabdophane to monazite-cheralite plus water ($\Delta H_{rh\rightarrow ch+H_2O}$) of the samples as obtained from TGA-DSC and drop solution calorimetry.

Composition	Water content	$\Delta H_{dehydr} \pm 2$ [kJ mol^{-1}]	$\Delta H_{transit} \pm 2$ [kJ mol^{-1}]	$\Delta H_{rh\rightarrow ch+H_2O}$ [kJ mol^{-1}]	
				DSC ± 2	Drop solution ± 1
$Pr_{0.892}Ca_{0.049}Th_{0.059}PO_4$	0.927	40.9	-25.3	-30	-29
$Pr_{0.785}Ca_{0.111}Th_{0.105}PO_4$	0.803	39.8	-21.3	-23	-21
$Pr_{0.697}Ca_{0.15}Th_{0.143}PO_4$	0.774	41.9	-25.8	-15	-18
$Nd_{0.804}Ca_{0.109}Th_{0.086}PO_4$	0.820	40.5	-32.7	-25	-23
	Average	40.8 ± 0.8			

3.2.2 Enthalpies of drop solution, formation from oxides and elements

The measured enthalpies of drop solution are listed in **Table 6** along with the values of enthalpy of formation from oxides and elements calculated using thermodynamic cycle provided in **Table 7**.

Table 6. Enthalpies of drop solution ($\Delta H_{ds,1073}$), formation from oxides ($\Delta H_{f\,ox,298}$) and from elements ($\Delta H_{f\,el,\,298}$) of monazite-cheralite and Th-rhabdophane samples (expressed in kJ mol^{-1}).

Composition	rhabdophanes			monazite-cheralites		
	$\Delta H^{rh}_{ds,1073}$	$\Delta H^{rh}_{f\,ox,\,298}$	$\Delta H^{rh}_{f\,el,\,298}$	$\Delta H^{ch}_{ds,1073}$	$\Delta H^{ch}_{f\,ox,298}$	$\Delta H^{ch}_{f\,el,298}$
$Pr_{0.892}Ca_{0.049}Th_{0.059}PO_4 \cdot 0.927H_2O$	206.64(7) ± 1.76	-297 ± 9	-2225 ± 9	167.28(6) ± 0.51	-326± 8	-1989 ± 9
$Pr_{0.785}Ca_{0.111}Th_{0.105}PO_4 \cdot 0.803H_2O$	200.46(7) ± 1.18	-297 ± 8	-2188 ± 9	162.64(6) ± 0.44	-318 ± 8	-1980 ± 8
$Pr_{0.697}Ca_{0.15}Th_{0.143}PO_4 \cdot 0.774H_2O$	197.26(9) ± 0.63	-293 ± 8	-2168 ± 8	158.62(7) ± 0.49	-311 ± 8	-1965 ± 8
$Nd_{0.804}Ca_{0.109}Th_{0.086}PO_4 \cdot 0.820H_2O$	195.86(8) ± 0.95	-295 ± 8	-2182 ± 9	158.79(6) ± 0.25	-317 ± 8	-1971 ± 8

Table 7. Thermodynamic cycle for calculation of enthalpy of formation from oxides, from elements and enthalpy of reaction of rhabdophane to cheralite-monazite plus water

Reaction	Enthalpy, [kJ mol^{-1}]
$Ln_{(1-x-y)}Ca_xTh_yPO_4 \cdot zH_2O_{(rh,298)} \rightarrow$ $\rightarrow 0.5(1-x-y)Ln_2O_{3(sln,1073)} + xCaO_{(sln,1073)} + yThO_{2(sln,1073)} + 0.5P_2O_{5\,(sln,1073)} + zH_2O_{(g,1073)}$	$\mathbf{\Delta H^{rh}_{ds,1073}}$ (see ***Table 6***)
$Ln_{(1-x-y)}Ca_xTh_yPO_{4\,(ch,298)} \rightarrow$ $\rightarrow 0.5(1-x-y)Ln_2O_{3(sln,1073)} + xCaO_{(sln,1073)} + yThO_{2(sln,1073)} + 0.5P_2O_{5\,(sln,1073)}$	$\mathbf{\Delta H^{ch}_{ds,1073}}$ (see ***Table 6***)
$Ln_2O_{3\,(s,298)} \rightarrow Ln_2O_{3\,(sln,1073)}$	$\mathbf{\Delta H_1(Nd) = 11.82 \pm 0.99}$ (Hosseini and Navrotsky, 2013) $\mathbf{\Delta H_1(Pr) = 16.50 \pm 0.20}$ (Zhang and Navrotsky, 2004)
$CaO_{(s,298)} \rightarrow CaO_{(sln,1073)}$	$\mathbf{\Delta H_2 = -7.08 \pm 2.31}$ (Cheng and Navrotsky, 2005)
$ThO_{2\,(s,298)} \rightarrow ThO_{2\,(sln,1073)}$	$\mathbf{\Delta H_3 = 98.10 \pm 1.70}$ (Mazeina et al., 2005)
$P_2O_{5\,(s,298)} \rightarrow P_2O_{5\,(sln,1073)}$	$\mathbf{\Delta H_4 = -342.1 \pm 7.9}$ (Popa et al., 2008)
$H_2O_{(l,298)} \rightarrow H_2O_{(g,1073)}$	$\mathbf{\Delta H_5 = 73.2}$ (Guo et al., 2015)
$2Ln_{(s,298)} + 1.5\,O_{2\,(g,298)} \rightarrow Ln_2O_{3\,(s,298)}$	$\mathbf{\Delta H_6(Nd) = -1806.9 \pm 3.0}$ (Navrotsky et al., 2015) $\mathbf{\Delta H_6(Pr) = -1809.9 \pm 3.3}$ (Navrotsky et al., 2015)
$2P_{(s,298)} + 2.5\,O_{2\,(g,298)} \rightarrow P_2O_{5\,(s,298)}$	$\mathbf{\Delta H_7 = -1504.9 \pm 0.5}$ (Robie and Hemingway, 1995)
$Ca_{(s,298)} + 0.5\,O_{2\,(g,298)} \rightarrow CaO_{(s,298)}$	$\mathbf{\Delta H_8 = -635.1 \pm 0.9}$ (Robie and Hemingway, 1995)
$Th_{(s,298)} + O_{2\,(g,298)} \rightarrow ThO_{2\,(s,298)}$	$\mathbf{\Delta H_9 = -1226.4 \pm 3.5}$ (Robie and Hemingway, 1995)
$H_{2\,(g,298)} + 0.5\,O_{2\,(g,298)} \rightarrow H_2O_{\,(s,298)}$	$\mathbf{\Delta H_{10} = -285.8 \pm 0.1}$ (Robie and Hemingway, 1995)
$0.5(1-x-y)Ln_2O_{3\,(s,298)} + xCaO_{(s,298)} + yThO_{2\,(s,298)} + 0.5P_2O_{5\,(s,298)} + zH_2O_{(l,298)} \rightarrow$ $\rightarrow Ln_{(1-x-y)}Ca_xTh_yPO_4 \cdot zH_2O_{(rh,298)}$	$\mathbf{\Delta H^{rh}_{f\,ox,298}}$ (see ***Table 6***)
$0.5(1-x-y)Ln_2O_{3\,(s,298)} + xCaO_{(s,298)} + yThO_{2\,(s,298)} + 0.5P_2O_{5\,(s,298)} \rightarrow$ $\rightarrow Ln_{(1-x-y)}Ca_xTh_yPO_{4\,(ch,298)}$	$\mathbf{\Delta H^{ch}_{f\,ox,298}}$ (see ***Table 6***)
$0.5(1-x-y)Ln_{(s,298)} + xCa_{(s,298)} + yTh_{(s,298)} + P_{(s,298)} + zH_{2\,(g,298)} + (2+0.5z)O_{2\,(g,298)} \rightarrow$ $\rightarrow Ln_{(1-x-y)}Ca_xTh_yPO_4 \cdot zH_2O_{(rh,298)}$	$\mathbf{\Delta H^{rh}_{f\,el,298}}$ (see ***Table 6***)
$0.5(1-x-y)Ln_{(s,298)} + xCa_{(s,298)} + yTh_{(s,298)} + P_{(s,298)} + 2O_{2\,(g,298)} \rightarrow$ $\rightarrow Ln_{(1-x-y)}Ca_xTh_yPO_{4\,(ch,298)}$	$\mathbf{\Delta H^{ch}_{f\,el,298}}$ (see ***Table 6***)
$Ln_{(1-x-y)}Ca_xTh_yPO_4 \cdot zH_2O_{(rh,298)} \rightarrow Ln_{(1-x-y)}Ca_xTh_yPO_{4\,(ch,298)} + zH_2O_{(l,298)}$	$\mathbf{\Delta H_{rh\rightarrow ch+H_2O}}$ (see ***Table 5***)

$$\Delta H^{rh}_{f\,ox,298} = -\Delta H^{rh}_{ds,1073} + 0.5 \times (1-x-y) \times \Delta H_1 + x \times \Delta H_2 + y \times \Delta H_3 + 0.5 \times \Delta H_4 + z \times \Delta H_5$$

$$\Delta H^{ch}_{f\,ox,298} = -\Delta H^{ch}_{ds,1073} + 0.5 \times (1-x-y) \times \Delta H_1 + x \times \Delta H_2 + y \times \Delta H_3 + 0.5 \times \Delta H_4$$

$$\Delta H^{rh}_{f\,el,298} = \Delta H^{rh}_{f\,ox,298} + 0.5 \times (1-x-y) \times \Delta H_6 + 0.5 \times \Delta H_7 + x \times \Delta H_8 + y \times \Delta H_9 + z \times \Delta H_{10}$$

$$\Delta H^{ch}_{f\,el,298} = \Delta H^{ch}_{f\,ox,298} + 0.5 \times (1-x-y) \times \Delta H_6 + 0.5 \times \Delta H_7 + x \times \Delta H_8 + y \times \Delta H_9$$

$$\Delta H_{rh\rightarrow ch+H_2O} = \Delta H^{rh}_{ds,1073} - \Delta H^{ch}_{ds,1073} - z \times \Delta H_5$$

The found values are plotted against ionic radius and compared to the results obtained for the rhabdophane end-member in Shelyug et al., (2018) (see **Figure 5**). For all samples in the current

study, enthalpies of drop solution are compatible to that of the $PrPO_4$ monazite-type end-member determined in the previous work (Shelyug et al., 2018). Nevertheless, the enthalpy of drop solution of the $Ca_{0.5}Th_{0.5}PO_4$ end-member determined by Popa et al., (2008) was (127.65 ± 4.4) kJ mol^{-1}. This value is 30 to 40 kJ mol^{-1} lower than the enthalpies of drop dissolution of the $Pr_{1-2x}Ca_xTh_xPO_4$ samples measured in this work. Additionally, a linear correlation between the enthalpies of drop solution and the ionic radius of cations was observed, where the ionic radii in the monazite-cheralites were the weighted averages of those of Ca^{2+}, Th^{4+}, and Pr^{3+} (**Table S4 of *Supporting Information***). A similar linear correlation was also observed for corresponding Th-rhabdophane $Pr_{1-2x}Ca_xTh_xPO_4{\cdot}nH_2O$, while their enthalpies of dissolution in the molten salt were more endothermic than those of the monazite-cheralite because of the evaporation of water.

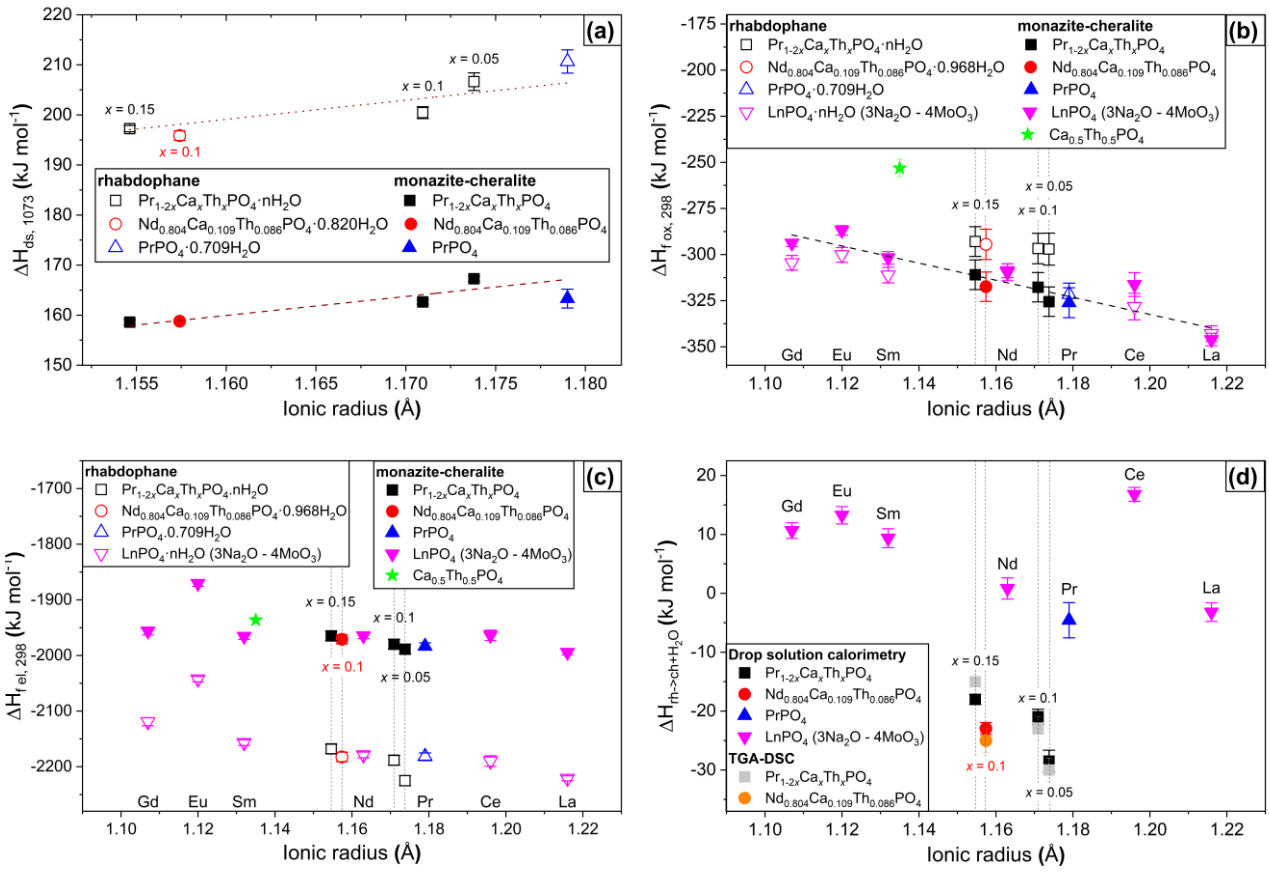

Figure 5. Evolution of enthalpies as a function of ionic radius: enthalpies of drop solution $\Delta H_{ds,1073\ K}$ (a), enthalpies of formation from oxides $\Delta H_{f\ ox,\ 298\ K}$ (b), and enthalpies of formation from elements $\Delta H_{f\ el,\ 298\ K}$ (c) and enthalpies of reaction of rhabdophane to cheralite-monazite plus water (d). The data of rhabdophanes are presented as open symbols and those of monazite-cheralite are closed symbols. The data of $LnPO_4$ and $Ca_{0.5}Th_{0.5}PO_4$ end-members are from (Shelyug et al., 2018) and (Popa et al., 2008), respectively.

Likewise, the enthalpies of formation from oxides or from elements of monazite-cheralite $Pr_{1-2x}Ca_xTh_xPO_4$ are in good agreement with those of monazite end-members $PrPO_4$, but lower than the enthalpy of formation of $Ca_{0.5}Th_{0.5}PO_4$. This result suggested the as-synthesized monazite-cheralite $Pr_{1-2x}Ca_xTh_xPO_4$ might be an ideal solid solution, but data obtained for samples at higher Th mole fractions are required to conclude definitely. On the contrary, the enthalpies of formation

from oxides of Th-rhabdophanes do not follow the trend of $LnPO_4 \cdot nH_2O$ series which might be the consequence of some additional interaction that should be taken into account.

3.3 Calculations on Gibbs free energy and entropies of formation associated with $Nd_{0.8}Ca_{0.10}Th_{0.10}PO_4 \cdot nH_2O$ and respective $Nd_{0.8}Ca_{0.10}Th_{0.10}PO_4$. Energetics of reaction of rhabdophane to cheralite-monazite plus water

The $\lg K^{\circ}_{s,0}$ value associated with reaction (21) was obtained from the solubility experiments and then was used to calculate the corresponding variation of Gibbs free energy, ΔG°_{r} at 298 K, according to equation (22):

$$Nd_{0.804}Ca_{0.109}Th_{0.086}PO_4 \cdot 0.820H_2O \leftrightarrow 0.804\ Nd^{3+} + 0.109\ Ca^{2+} + 0.086\ Th^{4+} + PO_4^{3-} + 0.820\ H_2O \quad (21)$$

$$\Delta G^{\circ}_{r} = -R \times T \times \ln K^{\circ}_{s,0} \quad (22)$$

where R is the gas constant and T the absolute temperature. Since $\lg K^{\circ}_{s,0}(\text{Th-rhabdophane}) \simeq \lg K^{\circ}_{s,0}(\text{monazite-cheralite})$, then $\Delta G^{\circ\,rh}_{r} = \Delta G^{\circ\,ch}_{r} = \Delta G^{\circ}_{r} = 178 \pm 2\ \text{kJ mol}^{-1}$.

Further, the variation of the standard Gibbs energy associated with the formation from the constitutive elements, $\Delta G_{f,el}$, was determined by applying the Hess's law and data from **Table S5** as follows:

$$\Delta G^{rh}_{f,el} = -\Delta G^{\circ}_{r} + 0.804 \times \Delta G^{\circ}_{f}(Nd^{3+}) + 0.109 \times \Delta G^{\circ}_{f}(Ca^{2+}) + 0.086 \times \Delta G^{\circ}_{f}(Th^{4+}) + \Delta G^{\circ}_{f}(PO_4^{3-}) + 0.82 \times \Delta G^{\circ}_{f}(H_2O) \quad (23)$$

$$\Delta G^{ch}_{f,el} = \Delta G^{\circ}_{r} + 0.804 \times \Delta G^{\circ}_{f}(Nd^{3+}) + 0.109 \times \Delta G^{\circ}_{f}(Ca^{2+}) + 0.086 \times \Delta G^{\circ}_{f}(Th^{4+}) + \Delta G^{\circ}_{f}(PO_4^{3-}) \quad (24)$$

Thus, the standard free energy of formation of the two phases differs by the value for water $0.820 \times \Delta G_{f,el}(H_2O) = -194.45 \pm 0.04\ \text{kJ mol}^{-1}$.

The entropies of formation from elements at 298 K were then calculated from:

$$\Delta S_{f,el} = \frac{\Delta H_{f,el} - \Delta G_{f,el}}{T} \quad (25)$$

Finally, the standard molar entropy, S_m°, could be expressed as follows:

$$S^{\circ}_{m}(rh) = \Delta S^{rh}_{f,el} + 0.804 \times S^{\circ}_{m}(Nd_{cr}) + 0.109 \times S^{\circ}_{m}(Ca_{cr}) + 0.086 \times S^{\circ}_{m}(Th_{cr}) + S^{\circ}_{m}(P_{cr}) + 2 \times S^{\circ}_{m}(O_{2\,g}) + 0.820 \times [0.5 \times S^{\circ}_{m}(O_{2\,g}) + S^{\circ}_{m}(H_{2\,g})] \quad (26)$$

$$S^{\circ}_{m}(ch) = \Delta S^{ch}_{f,el} + 0.804 \times S^{\circ}_{m}(Nd_{cr}) + 0.109 \times S^{\circ}_{m}(Ca_{cr}) + 0.086 \times S^{\circ}_{m}(Th_{cr}) + S^{\circ}_{m}(P_{cr}) + 2 \times S^{\circ}_{m}(O_{2\,g}) \quad (27)$$

Using the values listed in **Table S6** and the results of drop solution calorimetry from the previous section, the thermodynamic data for the rhabdophane and monazite-cheralite were calculated and summarized in **Table 8**.

Table 8. Thermodynamic data for $Nd_{0.8}Ca_{0.10}Th_{0.10}PO_4$ and $Nd_{0.8}Ca_{0.10}Th_{0.10}PO_4 \cdot 0.82H_2O$ (T = 298 K).

	$\Delta G_{f,el}$ [kJ mol^{-1}]	$\Delta S_{f,el}$ [J mol^{-1} K^{-1}]	$S_m°$ [J mol^{-1} K^{-1}]
$Nd_{0.804}Ca_{0.109}Th_{0.086}PO_4 \cdot 0.82\ H_2O$	-2059 ± 11	-413 ± 8	295 ± 9
$Nd_{0.804}Ca_{0.109}Th_{0.086}PO_4$	-1865 ± 11	-357 ± 7	161 ± 8

The Gibbs free energies of formation of some monazite end-members were determined before (Gavrichev et al., 2016; Gavrichev et al., 2009; Janots et al., 2007; Popa et al., 2006; Popa et al., 2008; Thiriet et al., 2005; Ushakov et al., 2001; Van Hoozen et al., 2020). The data obtained in the current study and the literature available data are provided in **Figure 6a** as a function of ionic radius. Similarly, **Figure 6b** presents the value of $\Delta G^{rh}_{f,el}$ determined in this work and those of rhabdophane end-members $LnPO_4 \cdot 0.667H_2O$, determined by Gausse et al., (2016) for the whole light lanthanide series. The difference between $\Delta G_{f,el}$ values of monazite compounds is smaller than that between those of rhabdophanes, nevertheless the coupled substitution of Nd by Th and Ca seems to stabilize both structures. The results depicted in **Figure S2** and **Figure S3** of ***Supporting Information***, suggest that monazite-cheralite and Th-rhabdophane solid solutions are stabilized by the configurational entropy term.

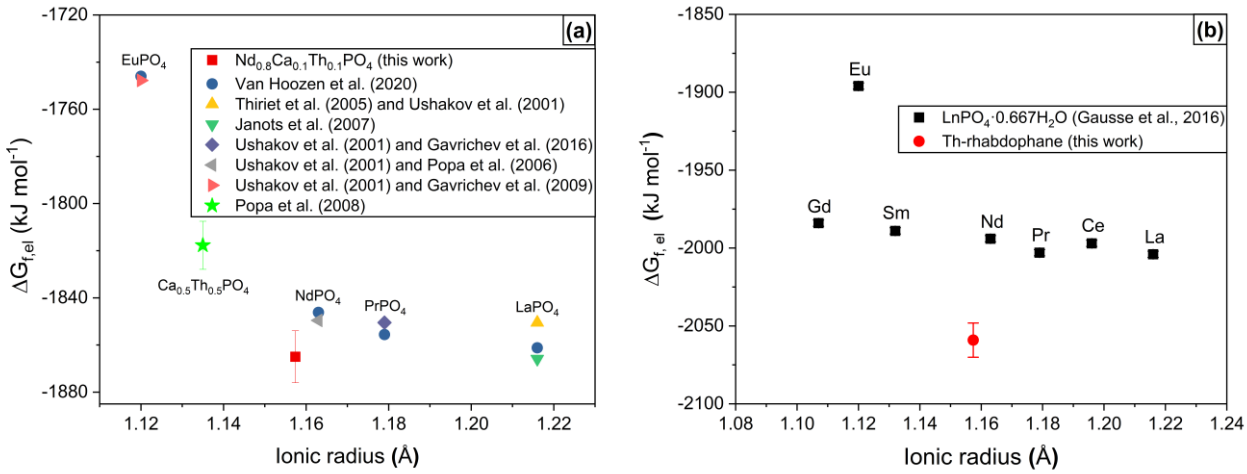

Figure 6. Evolution of Gibbs free energy of formation at 298 K as a function of ionic radius: monazite end-members/monazite-cheralite (a), rhabdophane end-members/Th-rhabodphane (b). Data from literature were cited from references (Gausse et al., 2016; Gavrichev et al., 2016; Gavrichev et al., 2009; Janots et al., 2007; Popa et al., 2006; Popa et al., 2008; Thiriet et al., 2005; Ushakov et al., 2001; Van Hoozen et al., 2020).

Finally, the entropy and Gibbs free energy of reaction (18) were calculated as follows:

$$\Delta S_{rh\rightarrow ch+H_2O} = -S_m^{rh} + S_m^{ch} + z \times S_m^{\circ}(H_2O) = -77 \pm 12 \text{ J mol K}^{-1} \quad (37)$$

$$\Delta G_{rh\rightarrow ch+H_2O} = \Delta H_{rh\rightarrow ch+H_2O} - 298.15 \times \Delta S_{rh\rightarrow ch+H_2O} = 0 \pm 5 \text{ kJ mol}^{-1} \quad (38)$$

These values imply that rhabdophane coexists with cheralite-monazite when it comes in contact with water at low temperature. Therefore, Th-rhabdophane $Nd_{0.8}Ca_{0.10}Th_{0.10}PO_4 \cdot nH_2O$ is the more probable solubility-controlling phase in this study, although the solubility products of the two phases were not significantly different considering the experimental uncertainty. Gausse et al., (2018) and Gausse et al., (2016) also concluded that rhabdophane was the solubility-controlling phase during the leaching of monazite end-members at low temperature (T < 383 K).

4 CONCLUSION

This work aimed to evaluate the chemical durability of monazite-cheralite $Ln_{1-2x}Ca_xTh_xPO_4$ (Ln = Pr, Nd; x = 0 – 0.15) converted from corresponding Th-rhabdophane $Ln_{1-2x}Ca_xTh_xPO_4 \cdot nH_2O$, which was prepared through wet chemistry synthesis.

Solubility experiments starting from under-saturated conditions were performed with $Nd_{0.8}Ca_{0.1}Th_{0.1}PO_4$ sample as an example of the series. When saturation conditions were reached, the associated standard solubility product was found as $\lg K_{s,0}^{\circ}$ = -31.2 ± 0.3, which implies virtually no Th release in solution at near neutral pH condition.

With the application of high temperature oxide melt solution calorimetry, the enthalpies of Th-rhabdophane and corresponding monazite-cheralite solid solutions were measured and thermodynamic parameters (ΔH_{ds}, $\Delta H_{f,ox}$, and $\Delta H_{f,el}$) were calculated. Combining these results with those of solubility experiments, the thermodynamic data associated with the formation of both phases from elements, ΔG_f°, ΔH_f° and ΔS_f°, were determined. Compared to the reported thermodynamic data of rhabdophane and monazite end-members, Th-rhabdophane $Nd_{0.8}Ca_{0.10}Th_{0.10}PO_4 \cdot nH_2O$ was found to be the more probable solubility-controlling phase at low temperature. Calculation of the thermodynamic data on reaction of Th-rhabdophane to cheralite-monazite plus water also supported the stability of the Th-rhabdophane phase.

This thermodynamic study of the Th-rhabdophane/monazite-cheralite system supports the high chemical durability of these solid solutions and confirm its potential as a specific conditioning matrix for the long-term immobilization of tetravalent actinides.

References

Boatner, L.A., 2002. Synthesis, Structure, and Properties of Monazite, Pretulite, and Xenotime. Reviews in Mineralogy and Geochemistry 48, 87-121. https://doi.org/10.2138/rmg.2002.48.4

Bruno, J., Bosbach, D., Kulik, D., Navrotski, A., 2007. Chemical Thermodynamics of Solid Solutions of Interest in Radioactive Waste Management. Chemical Thermodynamics 10, OECD Publishing.

Cheng, J., Navrotsky, A., 2005. Energetics of $La_{1-x}A_xCrO_{3-\delta}$ perovskites (A=Ca or Sr). Journal of Solid State Chemistry 178, 234-244. https://doi.org/10.1016/j.jssc.2004.11.028.

Ciavatta, L., 1980. The specific ion interaction theory in evaluating ionic equilibria. Annali Di Chimica 70, 551-567.

Clavier, N., 2004. Elaboration de phosphate-diphosphate de thorium et d'uranium (β-PDTU) et de matériaux composites β-PDTU/monazite à partir de précurseurs cristallisés.Etudes du frittage et de la durabilité chimique. Thèse de l'Université Paris Sud - Paris XI.

Clavier, N., Dacheux, N., Wallez, G., Quarton, M., 2006. Hydrothermal Methods as a New Way of Actinide Phosphate Preparation, Scientific Basis For Nuclear Waste Management XXX, Materials Research Society Symposium Proceedings 985, Boston, MA, 169.

Dacheux, N., Clavier, N., Podor, R., 2013. Versatile Monazite: Resolving geological records and solving challenges in materials science. Monazite as a promising long-term radioactive waste matrix: Benefits of high-structural flexibility and chemical durability. American Mineralogist 98, 833-847. https://doi.org/10.2138/am.2013.4307.

Delage, F., Dussossoy, J.L., 1990. R7T7 Glass Initial Dissolution Rate Measurements Using a High-Temperature Soxhlet Device, 14th International Symp On The Scientific Basis For Nuclear Waste Management. Materials Research Society Symposium Proceedings 212, Boston, MA, 41-47.

Du Fou de Kerdaniel, E., 2007. Etude de la dissolution de britholites et de solutions solides monazite/brabantite dopées avec des actinides. Thèse de l'Université Paris Sud-Paris XI.

Du Fou de Kerdaniel, E., Clavier, N., Dacheux, N., Podor, R., 2007a. Kinetic and Thermodynamic Study of the Chemistry of Neo-formed Phases During the Dissolution of Phosphate Based Ceramics, Scientific Basis For Nuclear Waste Management XXX. Materials Research Society Symposium Proceedings 985, Boston, MA, 341.

Du Fou de Kerdaniel, E., Clavier, N., Dacheux, N., Terra, O., Podor, R., 2007b. Actinide solubility-controlling phases during the dissolution of phosphate ceramics. Journal of Nuclear Materials 362, 451-458. https://doi.org/10.1016/j.jnucmat.2007.01.132.

Gausse, C., 2016. Synthèse et dissolution de matrices phosphatées de structure monazitique. Thèse de l'Université de Montpellier, p. 274.

Gausse, C., Szenknect, S., Mesbah, A., Clavier, N., Neumeier, S., Dacheux, N., 2018. Dissolution kinetics of monazite LnPO4 (Ln = La to Gd): A multiparametric study. Applied Geochemistry 93, 81-93. https://doi.org/10.1016/j.apgeochem.2018.04.005.

Gausse, C., Szenknect, S., Qin, D.W., Mesbah, A., Clavier, N., Neumeier, S., Bosbach, D., Dacheux, N., 2016. Determination of the Solubility of Rhabdophanes $LnPO_4 \cdot 0.667H_2O$ (Ln = La to Dy). European Journal of Inorganic Chemistry 2016, 4615-4630. https://doi.org/10.1002/ejic.201600517.

Gavrichev, K.S., Gurevich, V.M., Ryumin, M.A., Tyrin, A.V., Komissarova, L.N., 2016. Low-temperature heat capacity and thermodynamic properties of $PrPO_4$. Geochemistry International 54, 362-368. https://doi.org/10.1134/S001670291602004X.

Gavrichev, K.S., Ryumin, M.A., Tyurin, A.V., Gurevich, V.M., Komissarova, L.N., 2009. The heat capacity and thermodynamic functions of $EuPO_4$ over the temperature range 0–1600 K. Russian Journal of Physical Chemistry A 83, 901-906. https://doi.org/10.1134/S0036024409060053.

Giffaut, E., Grivé, M., Blanc, P., Vieillard, P., Colàs, E., Gailhanou, H., Gaboreau, S., Marty, N., Madé, B., Duro, L., 2014. Andra thermodynamic database for performance assessment: ThermoChimie. Applied Geochemistry 49, 225-236. https://doi.org/10.1016/j.apgeochem.2014.05.007.

Guo, X., Szenknect, S., Mesbah, A., Labs, S., Clavier, N., Poinssot, C., Ushakov, S.V., Curtius, H., Bosbach, D., Ewing, R.C., Burns, P.C., Dacheux, N., Navrotsky, A., 2015. Thermodynamics of formation of coffinite, $USiO_4$. Proceedings of the National Academy of Sciences of the United States of America 112, 6551-6555. https://doi.org/10.1073/pnas.1507441112.

Gysi, A.P., Harlov, D., Miron, G.D., 2018. The solubility of monazite ($CePO_4$), $SmPO_4$, and $GdPO_4$ in aqueous solutions from 100 to 250 °C. Geochimica et Cosmochimica Acta 242, 143-164. https://doi.org/10.1016/j.gca.2018.08.038.

Hirsch, A., Kegler, P., Alencar, I., Ruiz-Fuertes, J., Shelyug, A., Peters, L., Schreinemachers, C., Neumann, A., Neumeier, S., Liermann, H.P., Navrotsky, A., Roth, G., 2017. Structural,

vibrational, and thermochemical properties of the monazite-type solid solution $La_{1-x}Pr_xPO_4$. Journal of Solid State Chemistry 245, 82-88. https://doi.org/10.1016/j.jssc.2016.09.032.

Hosseini, S.M., Navrotsky, A., 2013. Energetic Effects of Substitution of La–Nd and Si–Ge Oxyapatite-Type Materials. Journal of the American Ceramic Society 96, 3915-3919. https://doi.org/10.1111/jace.12705.

Janots, E., Brunet, F., Goffé, B., Poinssot, C., Burchard, M., Cemič, L., 2007. Thermochemistry of monazite-(La) and dissakisite-(La): implications for monazite and allanite stability in metapelites. Contributions to Mineralogy and Petrology 154, 1-14. https://doi.org/10.1007/s00410-006-0176-2.

Johnson, J., Anderson, F., Parkhurst, D.L., 2000. Database thermo.com.V8.R6.230, Rev 1.11. , Lawrence Livermore National Laboratory, Livermore, CA.

Jonasson, R., Bancroft, G., Nesbitt, H.J.G.e.C.A., 1985. Solubilities of some hydrous REE phosphates with implications for diagenesis and sea water concentrations. Geochimica Et Cosmochimica Acta 49, 2133-2139. https://doi.org/10.1016/0016-7037(85)90071-7.

Lewis, G.N., Randall, M., Pitzer, K.S., Brewer, L., 1961. Thermodynamics. McGraw-Hill, New York.

Mazeina, L., Ushakov, S.V., Navrotsky, A., Boatner, L.A., 2005. Formation enthalpy of $ThSiO_4$ and enthalpy of the thorite -> huttonite phase transition. Geochimica Et Cosmochimica Acta 69, 4675-4683. https://doi.org/10.1016/j.gca.2005.03.053.

Mesbah, A., Clavier, N., Elkaim, E., Gausse, C., Kacem, I.B., Szenknect, S., Dacheux, N., 2014. Monoclinic Form of the Rhabdophane Compounds: $REEPO_4 \cdot 0.667H_2O$. Crystal Growth & Design 14, 5090-5098. https://doi.org/10.1021/cg500707b.

Montel, Kornprobst, Vielzeuf, 2000. Preservation of old U–Th–Pb ages in shielded monazite: example from the Beni Bousera Hercynian kinzigites (Morocco). Journal of Metamorphic Geology 18, 335-342. https://doi.org/10.1046/j.1525-1314.2000.00261.x.

Montel, J.-M., Razafimahatratra, D., Ralison, B., De Parseval, P., Thibault, M., Randranja, R., 2011. Monazite from mountain to ocean: a case study from Trolognaro (Fort-Dauphin), Madagascar. European Journal of Mineralogy 23, 745-757. https://doi.org/10.1127/0935-1221/2011/0023-2149.

Navrotsky, A., 1977. Progress and new directions in high temperature calorimetry. Physics and Chemistry of Minerals 2, 89-104. https://doi.org/10.1007/BF00307526.

Navrotsky, A., 2014. Progress and new directions in calorimetry: A 2014 perspective. Journal of the American Ceramic Society 97, 3349-3359. https://doi.org/10.1111/jace.13278.

Navrotsky, A., Lee, W., Mielewczyk-Gryn, A., Ushakov, S.V., Anderko, A., Wu, H.H., Riman, R.E., 2015. Thermodynamics of solid phases containing rare earth oxides. Journal of Chemical Thermodynamics 88, 126-141. https://doi.org/10.1016/j.jct.2015.04.008.

Neumeier, S., Kegler, P., Arinicheva, Y., Shelyug, A., Kowalski, P., Schreinemachers, C., Navrotsky, A., Bosbach, D., 2017. Thermochemistry of $La_{1-x}Ln_xPO_4$-monazites (Ln = Gd, Eu). Journal of Chemical Thermodynamics 105, 396. https://doi.org/10.1016/j.jct.2016.11.003.

Novotny, P., Sohnel, O., 1988. Densities of binary aqueous solutions of 306 inorganic substances. Journal of Chemical & Engineering Data 33, 49-55. https://doi.org/10.1021/je00051a018.

OECD/NEA, 1999. Geological Disposal of Radioactive Waste: Review of Developments in the Last Decade, Radioactive Waste Management. Paris. https://doi.org/10.1787/9789246180547-en.

Parkhurst, D.L., Appelo, C.A.J., 2013. Description of input and examples for PHREEQC version 3 - A computer program for speciation, batch-reaction, one-dimensional transport, and inverse geochemical calculations. U.S. Geological Survey Techniques and Methods, book 6, Chap. A43, available only at http://pubs.usgs.gov/tm/06/a43/, 497 p.

Popa, K., Jutier, F., Wastin, F., Konings, R.J.M., 2006. The heat capacity of $NdPO_4$. The Journal of Chemical Thermodynamics 38, 1306-1311. https://doi.org/10.1016/j.jct.2006.02.006.

Popa, K., Shvareva, T., Mazeina, L., Colineau, E., Wastin, F., Konings, R.J.M., Navrotsky, A., 2008. Thermodynamic properties of $CaTh(PO_4)_2$ synthetic cheralite. American Mineralogist 93, 1356-1362. https://doi.org/doi:10.2138/am.2008.2794.

Qin, D., Gausse, C., Szenknect, S., Mesbah, A., Clavier, N., Dacheux, N., 2017a. Solubility product of the thorium phosphate hydrogen-phosphate hydrate ($Th_2(PO_4)_2(HPO_4)\cdot H_2O$, TPHPH). Journal of Chemical Thermodynamics 114, 151-164. https://doi.org/10.1016/j.jct.2017.01.003.

Qin, D., Mesbah, A., Gausse, C., Szenknect, S., Dacheux, N., Clavier, N., 2017b. Incorporation of thorium in the rhabdophane structure: Synthesis and characterization of $Pr_{1-2x}Ca_xTh_xPO_4\cdot nH_2O$ solid solutions. Journal of Nuclear Materials 492, 88-96. https://doi.org/10.1016/j.jnucmat.2017.05.019.

Rand, M., Fuger, J., Grenthe, I., Neck, V., Rai, D., 2009. Chemical Thermodynamics of Thorium, Chemical Thermodynamics 11, OECD Publishing.

Robie, R.A., Hemingway, B.S., 1995. Thermodynamic properties of minerals and related substances at 298.15 K and 1 bar (10^5 pascals) pressure and at higher temperatures, U.S. Geological Survey Bulletin 2131.

Robisson, A.C., Dacheux, N., Aupiais, J., 2002. Influence of the pH on the dissolution of TPD and associated solid solutions. Journal of Nuclear Materials 306, 134-146. https://doi.org/10.1016/s0022-3115(02)01246-1.

Shelyug, A., Mesbah, A., Szenknect, S., Clavier, N., Dacheux, N., Navrotsky, A., 2018. Thermodynamics and Stability of Rhabdophanes, Hydrated Rare Earth Phosphates $REPO_4\cdot n H_2O$. Frontiers in Chemistry 6, 604. https://doi.org/10.3389/fchem.2018.00604.

Subramani, T., Rafiuddin, M.R., Shelyug, A., Ushakov, S., Mesbah, A., Clavier, N., Qin, D., Szenknect, S., Elkaim, E., Dacheux, N., Navrotsky, A., 2019. Synthesis, Crystal Structure, and Enthalpies of Formation of Churchite-type $REPO_4\cdot 2H_2O$ (RE = Gd to Lu) Materials. Crystal Growth & Design 19, 4641-4649. https://doi.org/10.1021/acs.cgd.9b00524.

Thiriet, C., Konings, R.J.M., Javorský, P., Magnani, N., Wastin, F., 2005. The low temperature heat capacity of $LaPO_4$ and $GdPO_4$, the thermodynamic functions of the monazite-type $LnPO_4$ series. Journal of Chemical Thermodynamics 37, 131-139. https://doi.org/10.1016/j.jct.2004.07.031.

Ushakov, S.V., Helean, K.B., Navrotsky, A., Boatner, L.A., 2001. Thermochemistry of rare-earth orthophosphates. Journal of Materials Research 16, 2623-2633. https://doi.org/10.1557/jmr.2001.0361.

Van Hoozen, C.J., Gysi, A.P., Harlov, D.E., 2020. The solubility of monazite ($LaPO_4$, $PrPO_4$, $NdPO_4$, and $EuPO_4$) endmembers in aqueous solutions from 100 to 250 °C. Geochimica et Cosmochimica Acta 280, 302-316. https://doi.org/10.1016/j.gca.2020.04.019.

Zhang, Y., Navrotsky, A., 2004. Thermochemistry of rare-earth aluminate and aluminosilicate glasses. Journal of Non-Crystalline Solids 341, 141-151. https://doi.org/10.1016/j.jnoncrysol.2004.04.027.

Acknowledgements

Ph.D. of Danwen Qin (ICSM) was funded by the China Scholarship Council (CSC).The authors thank Béatrice Baus-Lagarde (ICSM) for her contribution to ICP-OES analysis. The calorimetric studies were supported as part of the Materials Science of Actinides, an Energy Frontier Research Center funded by the U.S. Department of Energy, Office of Science, Basic Energy Sciences under Award Number DE-SC0001089. Anna Shelyug was funded in accordance with the state assignment by № AAAA-A19-119031890029-7 from the Ministry of Science and Higher Education of the Russian Federation.

Data availability

The research data is available upon request. To request the data, contact the corresponding author of the article.